

Physics-Aware Combinatorial Assembly Sequence Planning using Data-free Action Masking

Ruixuan Liu¹, Alan Chen², Weiye Zhao¹ and Changliu Liu¹

Abstract—Combinatorial assembly uses standardized unit primitives to build objects that satisfy user specifications. This paper studies assembly sequence planning (ASP) for physical combinatorial assembly. Given the shape of the desired object, the goal is to find a sequence of actions for placing unit primitives to build the target object. In particular, we aim to ensure the planned assembly sequence is physically executable. However, ASP for combinatorial assembly is particularly challenging due to its combinatorial nature. To address the challenge, we employ deep reinforcement learning to learn a construction policy for placing unit primitives sequentially to build the desired object. Specifically, we design an online physics-aware action mask that filters out invalid actions, which effectively guides policy learning and ensures violation-free deployment. In the end, we apply the proposed method to Lego assembly with more than 250 3D structures. The experiment results demonstrate that the proposed method plans physically valid assembly sequences to build all structures, achieving a 100% success rate, whereas the best comparable baseline fails more than 40 structures. Our implementation is available at <https://github.com/intelligent-control-lab/PhysicsAwareCombinatorialASP>.

Index Terms—Assembly, Task Planning, Reinforcement Learning, Robotics and Automation in Construction

I. INTRODUCTION

RECENT advancements in robot learning and control enable robots to perform various complex tasks, such as robotic assembly [1], [2], which is essential to automation in rapid prototyping, manufacturing, etc. Assembly sequence planning (ASP) is critical since a *physically feasible* action sequence should be planned beforehand in order for the agent, either a robot or a human, to successfully assemble the target object. Conventional assembly considers building the target object using unique components; thus, the goal is fixed, and the final component layout is known. Unlike conventional assembly, *combinatorial assembly* finds a feasible plan that uses standardized unit primitives to construct the goal object. Since the components are not unique, the final layout is undetermined. There could exist multiple permutations of the component layouts that construct the same structure, which significantly increases the problem complexity.

This paper studies combinatorial block assembly, which uses block primitives to assemble the target object. Combinatorial block assembly has been widely studied in numerous

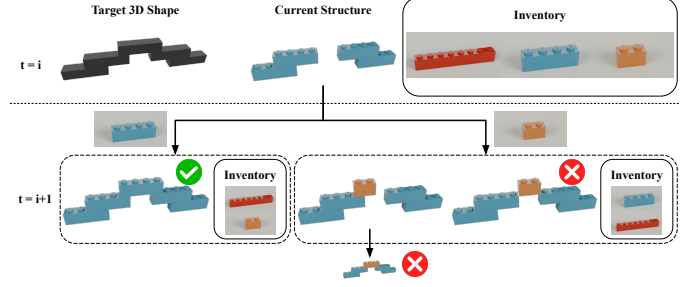


Fig. 1: Illustration of physics-aware combinatorial assembly.

fields, such as Lego construction [3], [4], warehousing [5], etc. In particular, this paper discusses combinatorial block assembly in the context of Lego assembly since it is a more complex sub-category of general combinatorial block assembly. Lego has been widely used in education [6] and assembly prototyping [7] since it allows users to freely customize the desired object. A Lego object is built using unit primitives, which are Lego bricks with a wide variety of different shapes. In particular, this paper adopts the setup in [1] where we build Lego objects using a limited inventory of standard Lego bricks on a $H \times W$ Lego base plate. Fig. 1 illustrates an example of combinatorial Lego ASP. Initially, only the shape of the goal object is given as well as an inventory of available bricks. Due to the combinatorial nature, there exist many options in designing the final brick layout as well as choosing the action sequence. At $t = i$, based on the target and current information, examples of a possible action could be placing a 1×4 brick or a 1×2 brick. The assembly is completed by placing a 1×4 brick as indicated by the green check mark in Fig. 1. On the other hand, there are multiple positions to place a 1×2 brick as shown in the bottom-right node in Fig. 1. The structure on the right is physically invalid since it would collapse after placing the brick. The structure on the left is valid. However, further expanding the assembly makes the layout physically invalid due to the inventory shortage.

Combinatorial ASP for Lego assembly is particularly challenging for several reasons. First, due to its combinatorial nature, the final assembly layout is undetermined, and thus, has multiple potential combinations and permutations of brick layouts that can build the desired object. It is difficult, if not impossible, to enumerate and search the full solution space. Second, the combinatorial nature leads to a large action space. As shown in Fig. 1, there exist numerous possible actions at a given step. Imagine building on a 48×48 Lego plate using 5 different types of bricks, there could be more than a million different actions that the agent can take. Note that this is already a simplified setting. There could be a lot more bricks

This work is in part supported by the Manufacturing Futures Institute, Carnegie Mellon University, through a grant from the Richard King Mellon Foundation.

¹Ruixuan Liu, Weiye Zhao and Changliu Liu are with Robotics Institute, Carnegie Mellon University, Pittsburgh, PA, USA. ruixuanl@cmu.edu, weiyezha@cmu.edu, cliu6@andrew.cmu.edu

²Alan Chen is with Westlake High School, Austin, TX, USA.

and a larger workspace in reality, which would further enlarge the action space and increase problem complexity. Third, combinatorial ASP requires the agent to plan its actions sequentially, and the long time horizon significantly increases the problem complexity. The agent needs to have a comprehensive understanding of the structure since an inappropriate action taken earlier could implicitly harm the assembly multiple steps later. Fourth, the planned sequence should be physically valid in order to be executed in reality. For example, the right action of placing a 1×2 brick in Fig. 1 is physically invalid since the structure will collapse. The left action of placing a 1×2 brick causes a dead end since the inventory is insufficient. These physical constraints are important for real assembly but are generally difficult to encode.

To address the above-mentioned challenges, this paper employs deep reinforcement learning (RL) to learn a sequential construction policy for placing unit primitives to build the desired object. Specifically, we use a neural network (NN) to capture the structural information and approximate the construction policy. To ensure physical validity, we design an online action mask that filters invalid actions and guides policy learning. Finally, we demonstrate that the proposed method successfully learns to generate a physically valid assembly sequence for constructing the target object. The generated construction plan can be executed in real. Our contributions are summarized as follows:

- 1) We propose an RL framework to address combinatorial ASP effectively.
- 2) We design an online action mask to integrate physical constraints, which effectively guides policy learning and ensures violation-free deployment. The action mask is data-free and does not require a physics engine.
- 3) We demonstrate executing the planned assembly sequences by both humans and robots. The experiment shows that the proposed method can generate physically valid assembly sequences for combinatorial assembly.

The rest of this paper is organized as follows: Sec. II discusses relevant works. Sec. III introduces our proposed physics-aware combinatorial ASP and Sec. IV demonstrates experiment results. Sec. V discusses potential extensions, as well as limitations and future works. Sec. VI concludes the paper.

II. RELATED WORKS

Assembly sequence planning has been widely studied [8], [9]. Conventional assembly considers assembling a target object using unique components, resulting in a fixed initial state and a fixed goal state. Thus, previous works [10], [11], [12] plan the assembly sequence by disassembling the goal object. Since states in ASP are commonly represented as graphs, recent works [13], [14], [15] employ graph neural networks to model the construction policy by capturing the relations between components. Due to the discrete nature of ASP, [10], [16] formulate the problem as an optimization problem and solve it using integer linear programming (ILP).

Combinatorial assembly is a special category of assembly, in which the goal state is not fully constrained and multiple permutations of unknown goal states exist. Combinatorial ASP

can be seen in numerous fields. In the biological field, [17] studies combinatorial assembly for designing enzymes with diverse, low-energy structures and stable catalytic constellations. Combinatorial assembly is also widely applied in physical construction [18], where people use unit primitives to construct objects to satisfy certain constraints (*e.g.*, shape). In addition, in warehousing, [5] uses unit primitives, *i.e.*, package boxes, to maximize space utilization in palletization. Besides, combinatorial assembly is also common in prototyping, *e.g.*, Lego prototyping [7] in which people use unit primitives, *i.e.*, Lego bricks, to assemble a desired prototyping object. Previous works [19], [3] study brick layout optimization for a given structure. Given an optimized and fixed target brick layout, the combinatorial ASP can be treated as conventional ASP. However, optimizing the brick layout itself is challenging. [4] tackles combinatorial ASP using deep RL. With the success of AlphaGo [20], recent works [21], [22], [23] adopt the combination of RL and tree search to solve ASP.

Recent efforts have been focusing on encoding physics constraints when generating the assembly plan. With the advancements in the physics engine, [24], [23], [11], [5] leverage simulators to guide ASP. However, Lego structures have complex interlocking connections. To our knowledge, no existing simulators can reliably simulate the connections between Lego bricks. Due to the lack of simulators, [24] assumes the assembled structure is a rigid whole body and only validates whether the structure can stand still.

III. PHYSICS-AWARE COMBINATORIAL ASSEMBLY SEQUENCE PLANNING

In this section, we introduce our proposed method for physics-aware combinatorial ASP. We consider the input as a user-specified voxelized 3D shape within a $H \times W \times D$ workspace. Due to its discrete nature, an input shape can be represented as $\mathcal{V}_T \in \mathbb{R}^{H \times W \times D}$. In addition, we have N different types of unit primitives. Fig. 2 illustrates an overview of the proposed physics-aware ASP method, which will be detailed in the following sections.

A. Problem Formulation

Given the target shape \mathcal{V}_T , we aim to construct an object that minimizes the difference to the goal object, by a sequence of actions. Only one component can be placed at each step as illustrated in Fig. 1. This paper formulates the combinatorial ASP as a Markov decision process, which is denoted as $\mathcal{M} = (\mathcal{S}, \mathcal{A}, \mathcal{P}, \mathcal{R})$, where \mathcal{S} denotes the state space and \mathcal{A} represents the action space. $\mathcal{P} : \mathcal{S} \times \mathcal{A} \rightarrow \mathcal{S}$ is the transition function between states caused by an action. $\mathcal{R} : \mathcal{S} \times \mathcal{A} \rightarrow \mathbb{R}$ denotes the reward function, which outputs a real-valued reward for taking an action. In a standard RL framework, the objective is to find a policy, $\pi(a_t|s_t)$, that maximizes the accumulated discounted reward $J(\pi) = \mathbb{E}[\sum_{t=0}^T \gamma^t r_t]$, where $r \in \mathcal{R}$ and $\gamma \in [0, 1)$ is a discount factor.

a) *State*: At a given time step $t \in [0, T]$, the state is represented as $s_t = (\mathcal{V}_t, \mathcal{V}_t, G_t, \mathcal{I}_t)$ as shown in the left in Fig. 2. \mathcal{V}_t is the current shape being assembled. $G_t = \{a_0, a_1, \dots, a_{t-1}\}$ is the graph tracking all bricks being

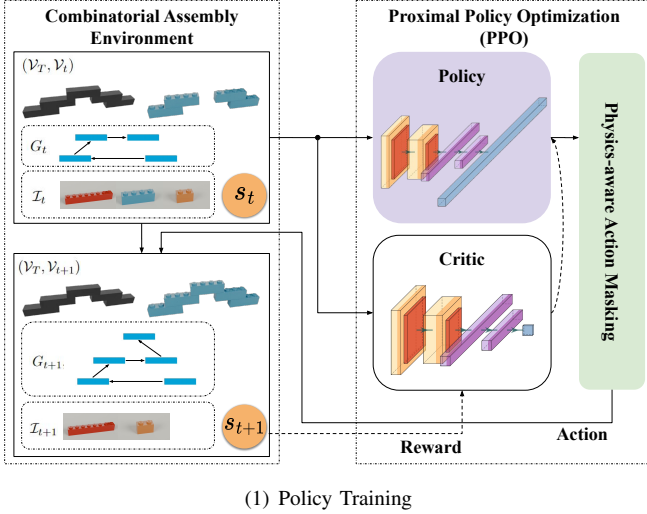


Fig. 2: Overview of the proposed physics-aware ASP pipeline. In policy training, the physics-aware action mask filters out invalid actions and guides policy learning. The agent interacts with the environment by sampling actions from the masked policy distribution and learns from the reward feedback. In policy deployment, the action is selected by maximum likelihood on the masked policy distribution to ensure violation-free deployment.

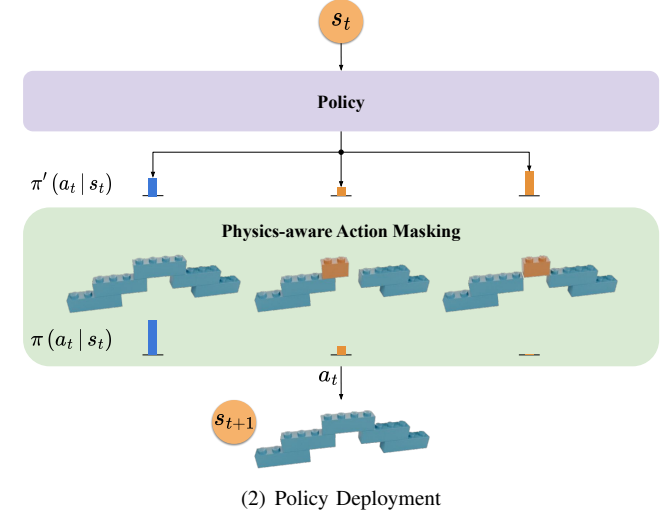
assembled, where a_i denotes the action of placing a brick at step i . In addition, the state also tracks the brick inventory $\mathcal{I}_t \in \mathbb{N}^N$. The inventory indicates available bricks that can be used as shown on the left in Fig. 2. Note that due to the combinatorial nature, G_t is not unique given \mathcal{V}_t , and thus, we track G_t explicitly in the state.

b) Action: We define the action as placing a unit primitive onto the structure in progress. At each time step, the policy π needs to output three decisions, 1) selecting a brick $b_t \in [1, 2, \dots, N]$, 2) placing it at position $p_t = (x_t, y_t, z_t)$, where $x_t \in [1, 2, \dots, H], y_t \in [1, 2, \dots, W], z_t \in [1, 2, \dots, D]$, and 3) rotating it to the proper orientation $\omega_t \in [0, 1]$, where 0 denotes the landscape orientation and 1 indicates the portrait orientation. Therefore, we have the action defined as $a_t = (b_t, p_t, \omega_t)$. The action space is of a combinatorial nature since at a given step, the agent can place any brick at any grid on board with any orientation. As a result, we have a combinatorial action space with the dimensionality of $H \times W \times D \times N \times 2$, which can easily lead to more than a million possible actions at a given time step.

c) Transition: Given the state s_t , the transition function determines the next state s_{t+1} with the given action a_t . Note that the target \mathcal{V}_T in s_t and s_{t+1} will remain the same as illustrated in Fig. 2. The brick graph G_{t+1} is updated as $G_{t+1} = G_t \cup a_t$. Given G_{t+1} , the next step structural shape \mathcal{V}_{t+1} is uniquely defined. The brick inventory will be updated as $\mathcal{I}_{t+1}^b = \mathcal{I}_t^b - 1$, whereas the other entries remain the same as shown in the left in Fig. 2.

d) Reward: The goal for ASP is to construct an object \mathcal{V}_t that fills up the target shape \mathcal{V}_T . Thus, we define the accumulated reward as a measure of the space utilization of the target. The instant and terminal rewards can be written as

$$r(a_t, s_t) = \frac{(\mathcal{V}_{t+1} - \mathcal{V}_t) \cap \mathcal{V}_T}{\mathcal{V}_T}, \quad r_T = \begin{cases} 0, & \text{if succeeds.} \\ -\infty, & \text{if fails.} \end{cases} \quad (1)$$



The terminal reward r_T penalizes the agent if it violates physical constraints or fails. Note that the reward in Eq. (1) denotes a minimal form, which does not include sophisticated punishment and leads to a standardized accumulated reward, *i.e.*, $J(\pi) = 1$ when the assembly succeeds and $\gamma = 1$.

B. Physics-aware Action Masking

This paper emphasizes the physical feasibility of the planned assembly sequence. Conventional RL approaches integrate constraints into Eq. (1) by designing more sophisticated r and r_T , *e.g.*, reduced reward when executing a sub-optimal action, punishment when violating physics constraints. However, integrating constraints into the reward function is usually time-consuming and does not guarantee violation-free deployment.

Action masking [25] is a widely used technique in RL to address large discrete action space. Due to the nature of combinatorial ASP, we integrate constraints by designing an online physics-aware action mask. At a given time t , the policy outputs the action distribution $\pi'(a_t | s_t)$ as shown in Fig. 2. The online action mask verifies the action validity as

$$M(a_t | s_t) = \begin{cases} 1, & \text{if } a_t \text{ is physically valid.} \\ 0, & \text{otherwise.} \end{cases} \quad (2)$$

The final policy distribution is calculated as $\pi(a_t | s_t) \sim \pi'(a_t | s_t) \cdot M(a_t | s_t)$. An example of the action masking is illustrated on the right of Fig. 2. Since placing a floating 1×2 (*i.e.*, orange) brick would generate a collapsing structure, the physics-aware action mask identifies it as an invalid operation and suppresses the action probability. During the training phase, the agent updates the policy based on the masked distribution $\pi(a_t | s_t)$. [25] has shown that the gradient produced by masking out invalid actions remains a valid policy gradient, which can be used to learn the action policy. During the deployment phase, the policy outputs the masked distribution $\pi(a_t | s_t)$ for execution. With the physics-aware action mask, the action space can be significantly reduced, making the exploration and learning more efficient. Moreover,

the action mask encodes physics as a hard constraint, which guarantees physical feasibility during deployment. We consider the following aspects to ensure the physical feasibility of the planned assembly sequence.

a) Task-oriented: The goal of combinatorial ASP is to build a structure that replicates the desired shape. Thus, placing bricks outside the shape does not contribute to the task. To ensure that the action is task-oriented, we have

$$T(a_t|s_t) = \begin{cases} 1, & \text{if } (\mathcal{V}_{t+1} - \mathcal{V}_t) \cap \mathcal{V}_T = (\mathcal{V}_{t+1} - \mathcal{V}_t). \\ 0, & \text{otherwise.} \end{cases} \quad (3)$$

b) Collision-free: When performing physical assembly, one cannot place a unit primitive that collides with the existing structure. To ensure collision-free assembly, we enforce

$$C(a_t|s_t) = \begin{cases} 1, & \text{if } (\mathcal{V}_{t+1} - \mathcal{V}_t) \cap \mathcal{V}_t = \emptyset. \\ 0, & \text{otherwise.} \end{cases} \quad (4)$$

c) Inventory: In real assembly, the user can only choose available primitives to assemble the structure. We enforce the inventory constraint as

$$I(a_t|s_t) = \begin{cases} 1, & \text{if } \mathcal{I}_t^{b_t} > 0. \\ 0, & \text{otherwise.} \end{cases} \quad (5)$$

d) Operability: To accomplish physical assembly, it is important to ensure that each planned action a_t is physically operable. Due to the nature of Lego assembly (*i.e.*, the knob-to-cavity connections), a vertical motion for insertion is required to assemble a brick. Thus, a brick can only be assembled when either the top or bottom is unoccupied. We enforce the operability constraint as

$$O(a_t|s_t) = \begin{cases} 1, & \text{if } V^+(a_t) = 0 \vee V^-(a_t) = 0. \\ 0, & \text{otherwise.} \end{cases} \quad (6)$$

V^+ and V^- measures the occupancy of the region one layer above and below the action a_t . Essentially, the operability ensures that when assembling a_t , either its top or bottom is empty so that there is enough room for brick insertion.

e) Structural Stability: It is important to ensure that after the agent performs the assembly action, the resulting structure does not collapse. Specifically, the goal is to ensure that $\forall t \in [0, T]$, G_t is stable, *i.e.*, statically stable. However, it is practically impossible to try each of the actions to build the structures and observe the resulting stability manually. Recent works [23], [5] leverage physics engines to simulate structural stability. However, Lego assembly has a more complex interlocking mechanism and existing simulators cannot reliably capture the static structural stability.

To address the challenge, we leverage the optimization-based analysis in [26] to effectively estimate the structural stability. Given a Lego structure G_t , we derive the simplified force model and solve a force distribution by optimizing over force balancing equations. For each assembled brick a_i , a corresponding stability score $v_i \in [0, 1]$ can be calculated, which indicates the internal stress level in the brick connection.

A larger v_i indicates higher internal stress and the connection is more likely to break. We define the stability constraint as

$$S(a_t|s_t) = \begin{cases} 1, & \text{if } v_i < 1, \forall i \in [0, t]. \\ 0, & \text{otherwise.} \end{cases} \quad (7)$$

Combining all the constraints, the physics-aware action mask Eq. (2) can be defined as

$$M(a_t|s_t) = \begin{cases} 1, & \text{if } T \wedge C \wedge I \wedge O \wedge S. \\ 0, & \text{otherwise.} \end{cases} \quad (8)$$

Note that Eq. (8) denotes the minimal form of the action mask required for generating physically valid assembly sequences for human operators, or robots capable of performing human-level manipulation. However, existing robots are usually not as dexterous as humans. Thus, we further consider the robot constraints as follows.

f) Robot Manipulability: To allow robots to perform the assembly physically, it is critical to ensure that 1) the robots have enough space to perform the necessary assembly motion, and 2) the assembly operation would not collapse the structure. We use $\mathcal{V}_R^{a_t}$ to denote the total volume occupied by the robotic system to perform the assembly step a_t and $S_R^{a_t}$ to denote the structural stability under the robot impact, *i.e.*, dynamic stability. $S_R^{a_t} = 1$ indicates that the structure can withstand the operation and $S_R^{a_t} = 0$ denotes that the structure will collapse. The constraint can be defined as

$$U(a_t|s_t) = \begin{cases} 1, & \text{if } \mathcal{V}_t \cap \mathcal{V}_R^{a_t} = \emptyset \wedge S_R^{a_t} = 1. \\ 0, & \text{otherwise.} \end{cases} \quad (9)$$

Note that Eq. (9) heavily depends on the task and the robot's capability. For instance, in the case of palletization with a suction gripper, $\mathcal{V}_R^{a_t}$ only includes the volume above a_t since the suction gripper does not occupy areas adjacent to a_t . $S_R^{a_t}$ is reduced to $S(a_t|s_t)$ since it is a simple placing motion. In the case of palletization with a parallel gripper, $\mathcal{V}_R^{a_t}$ would include additional volumes adjacent to a_t to account for the gripper geometry. Nevertheless, $S_R^{a_t}$ can still be reduced to $S(a_t|s_t)$ since no additional impact will be exerted on the structure. In the case of Lego assembly, $S_R^{a_t}$ would be different since the robot needs to force the knobs into the cavities to establish the connection, which would exert extra forces on the structure and additional support might be necessary. Consequently, $\mathcal{V}_R^{a_t}$ includes not only the volume of the gripper but also volumes for the robot to operate as well as the volume occupied due to additional support. More details on determining $\mathcal{V}_R^{a_t}$ and $S_R^{a_t}$ for the robotic system we use are discussed in Sec. IV-D.

Combining all the constraints, the physics-aware action mask for robots can be defined as

$$M_R(a_t|s_t) = \begin{cases} 1, & \text{if } T \wedge C \wedge I \wedge O \wedge S \wedge U. \\ 0, & \text{otherwise.} \end{cases} \quad (10)$$

As shown in Fig. 2, the proposed physics-aware action mask, either Eq. (8) or Eq. (10), is applied in both the training and deployment phases. During policy training, the action mask filters out invalid actions and the action is sampled from the masked policy distribution, *i.e.*, a reduced action space. During policy execution, the action a_t is generated by

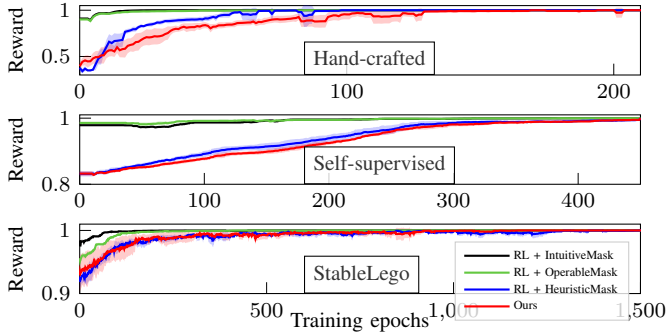


Fig. 3: Training rewards for different methods on different evaluation sets.

maximum likelihood on the masked policy distribution π . Note that, unlike prior works that require a massive dataset to train the action mask or physics engines to generate feedback, the presented action mask can be numerically computed.

IV. EXPERIMENTS

The proposed physics-aware ASP is applied to Lego assembly to demonstrate its effectiveness in combinatorial assembly. In our experiment, we have a limited brick inventory, which includes 8 types of bricks, *i.e.*, 1×1 , 1×2 , 1×4 , 1×6 , 1×8 , 2×2 , 2×4 , and 2×6 . Due to the limited inventory, it is important to ensure that the testing 3D shapes indeed have feasible assembly sequence solutions. Thus, we evaluate in four assembly scenarios, *i.e.*, 1) hand-crafted shapes, 2) self-supervised generated shapes, 3) designs in StableLego [26], and 4) more difficult designs in StableLego (*i.e.*, Hard StableLego). Table. II lists the number of shapes in each scenario. We use the shape volume C_v and the unsupported ratio C_s to quantitatively estimate the difficulty of a given 3D shape. In particular, we have the two metrics defined as $C_v = N_{V_T}$ and $C_s = \frac{N_{\emptyset}}{N_{V_T}}$, where N_{V_T} is the number of voxels in the shape, and N_{\emptyset} denotes the number of voxels that are not directly connected to the ground. In general, a larger C_v indicates a longer horizon planning task. A larger C_s indicates that the structure is more likely to experience high internal stress, and thus, requires a more sophisticated layout design to ensure physical buildability. Due to the limitation of the manipulation capability, not all Lego structures are buildable by robots. Thus, the following experiments are conducted with the action mask in Eq. (8) to demonstrate the capability of our method to generate physically valid assembly sequences for human users. The experiment for generating robot-capable assembly sequences is in Sec. IV-D.

To demonstrate the physics awareness of the proposed method (RL + FullMask), we compare it to several baselines 1) Vanilla RL, 2) RL + IntuitiveMask, 3) RL + OperableMask, 4) RL + HeuristicMask. Besides, we also compare our method to search-based baselines, which use Monte-Carlo Tree Search (MCTS), including 5) MCTS + IntuitiveMask, 6) MCTS + OperableMask, 7) MCTS + HeuristicMask, and 8) MCTS + FullMask. The Vanilla RL integrates constraints into the reward function. If either C , I , O , or S is violated, the rollout is terminated and the agent is punished by the terminal reward r_T . Otherwise, the instant reward is calculated as shown in Eq. (1). The **IntuitiveMask** is a simplified action

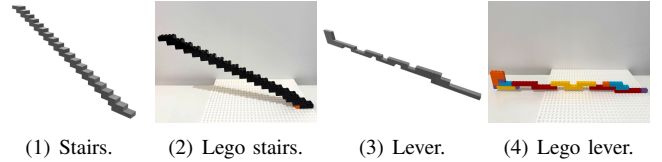


Fig. 4: Example hand-crafted shapes and their planned assemblies in real.

TABLE I: PPO hyperparameters.

Steps per Update	Batch Size	Epochs	Entropy Coefficient
256	32	4	0.1
λ_{gae}	γ	Clip Range	Value Coefficient
0.95	0.95	0.5	1

mask, which only includes T, C, I , since they are the most intuitive constraints. Similarly, the **OperableMask** adopts an action mask that includes T, C, I, O . The **HeuristicMask** uses an action mask that includes T, C, I, O, S . But instead of computing S by solving the optimization in Eq. (7), it uses a heuristic to infer the structural stability. In particular, the heuristic we use is that the structure is stable if, for all bricks in the assembly, there exists a connected path to the ground. This is a widely used heuristic in Lego layout optimization [19]. The **FullMask** denotes the proposed action mask in Eq. (8). For RL-based baselines, the different masks guide the policy learning and inference, while for the search-based baselines, the masks prune the tree branches to reduce the search space. For all methods, we constrain the agent to finish the assembly within 60 steps. All search-based methods have 100 look-ahead steps. Note that we do not include the vanilla MCTS because the time for making a decision is too long ($> 10\text{min}$) due to the large search space. All RL-based methods are implemented using Stable-Baselines3 [27] and trained using Proximal Policy Optimization (PPO) [28] with the learning rate being $3e^{-4}$. The hyperparameters are listed in Table. I. We use an identical NN structure for all the RL-based methods, which includes 2 convolutional layers with the kernel size being 5 and output channels being 8 and 32, followed by 2 fully connected layers with 512 and 128 hidden neurons. All layers have the Tanh activation. We repeat the experiments with five different random seeds, and the training profiles are shown in Fig. 3. The reward profile of vanilla RL is not shown since it struggles to learn at all (*i.e.*, < 0.01) due to the enormous exploration space, while other methods effectively learn and accomplish the assembly in a way that satisfies their constraints (*i.e.*, reward reaches 1). Note that despite satisfying their own constraints, it does not necessarily mean that the planned assembly can be performed in real.

A. Hand-crafted Shapes

We manually design 10 3D shapes to validate the performance of the proposed method. Fig. 4 showcases examples of the hand-crafted shapes. To emphasize physics awareness, we intentionally design these shapes to be more difficult, *i.e.*, having larger sizes, and more overhanging structures, which is also indicated by C_v and C_s in Table. II. For all methods, we manually verify the planned sequences and display the physical success rate in Table. II. Despite the baselines accomplishing the assemblies in training as shown in Fig. 3,

TABLE II: Evaluation datasets and the corresponding success rates for different methods when executing in real.

Number of 3D Shapes		Hand-crafted	Self-supervised	StableLego [26]	Hard StableLego [26]
		10	150	100	20
Shape Complexity	C_v (Avg, Std)	(96.3, 43.8)	(42.5, 23.9)	(67.0, 28.9)	(68.4, 32.3)
	C_s (Avg, Std)	(0.717, 0.225)	(0.280, 0.230)	(0.262, 0.279)	(0.647, 0.206)
Search-based	MCTS + IntuitiveMask	0%	32.7%	27%	0%
	MCTS + OperableMask	40%	70%	54%	10%
	MCTS + HeuristicMask	20%	91.3%	80%	50%
	MCTS + FullMask	40%	91.3%	79%	60%
RL-based	Vanilla RL	0%	0%	0%	0%
	RL + IntuitiveMask	0%	22.7%	18%	0%
	RL + OperableMask	0%	26.7%	34%	0%
	RL + HeuristicMask	30%	92.7%	80%	70%
	Ours (RL + FullMask)	100%	100%	100%	100%

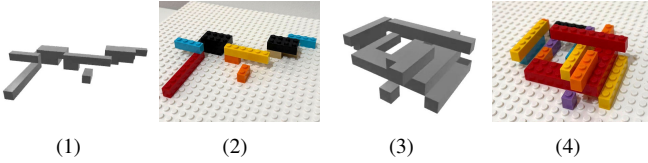


Fig. 5: Examples of self-supervised shapes and their real assemblies.

their planned assembly sequences are not always physically executable due to the mismatch between computation and real-world physics. Moreover, since these hand-crafted shapes require more sophisticated layout designs, all baselines result in their worst performance among all evaluation sets. MCTS + FullMask achieves the best success rate among all baselines. All actions planned by MCTS + FullMask are physically valid, which demonstrates the effectiveness of the proposed action mask. However, due to the long horizon of the planning problem, it fails the majority of the testing samples due to entering dead-end states with no available actions as shown in Fig. 7(3). On the other hand, the proposed method can find physically valid assembly sequences for all the samples.

B. Self-supervised Shape Generation

It is difficult, if not impossible, to massively design 3D shapes by hand that have physically valid assembly sequences. Therefore, we leverage the action mask in Eq. (8) to auto-generate 3D shapes as shown in Fig. 5(1) and 5(3). For each step t , we randomly pick an action a_t such that $M(a_t|s_t) = 1$ and $|x_t - x_{t-1}| \leq \epsilon_x$, $|y_t - y_{t-1}| \leq \epsilon_y$, where ϵ_x and ϵ_y are user-specified offsets. ϵ_x and ϵ_y encourage consecutive actions to be close instead of having a scattered structure. Specifically, we set $\epsilon_x = 2$, $\epsilon_y = 2$ and randomly generate 150 3D shapes ranging from 1-30 steps. Despite the diverse 3D shapes, the C_v and C_s in Table. II indicate that these auto-generated shapes are easier since they have more supportive structures. Thus, we can see the baselines generally achieve higher success rates, but still fail a lot, as shown in Table. II. The proposed method outperforms the baselines and successfully plans physically valid assembly sequences for all the structures.

C. StableLego Shapes

StableLego [26] is a large-scale dataset that contains the brick layouts for different objects. It contains a mixture of stable and unstable Lego designs. We randomly sampled 100 stable designs and 20 unstable designs (*i.e.*, Hard StableLego) from a subset (*i.e.*, < 50 bricks) of StableLego. To ensure that

the shapes are physically buildable, we manually verify that a feasible assembly sequence exists for each shape in the hard set. As indicated by C_s in Table. II, the Hard StableLego is generally more difficult than the regular set since there are more overhanging structures. As a result, the baselines generally achieve higher success rates in the regular set than in the hard set. Nevertheless, the proposed method outperforms the baselines and finds physically executable assembly sequences for all the shapes.

The action mask in Eq. (8) ensures the assembly action 1) contributes to the task, 2) is collision-free, 3) has sufficient inventory, 4) is operable, and 5) will result in a stable next-step structure. Thus, the assembly sequence is physically executable. Fig. 4 to 6 demonstrate the resulting assemblies¹ performed by a human following the planned sequences.

D. Robot Execution

To plan robot-executable assembly sequences, we employ the action mask in Eq. (10). Specifically, we use the bimanual system in Fig. 9, and the robots' motion is planned and executed using [29], [30]. We model the robot operation for executing a_t (*i.e.*, forcing brick connections) as a virtual brick $a'_t = (b_t, x_t, y_t, z'_t, \omega_t)$ with heavier weight, *e.g.*, 1kg. $z'_t = z_t + 1$ if the robot grabs the brick from the top and $z'_t = z_t - 1$ if the robot grabs it from the bottom. The dynamic stability for assembling a_t is equivalent to the static stability of the structure $G'_t = G_t \cup a_t \cup a'_t$, which can be evaluated following Eq. (7). G'_t being stable indicates that no additional support is needed when performing a_t . Otherwise, additional support is needed to execute a_t . To find valid support, we search for a virtual supporting brick $a^*_t = (b_t, x^*_t, y^*_t, z^*_t, \omega_t)$ with negative weight as a'_t , such that the virtual structure $G^*_t = G'_t \cup a^*_t$ is stable. Thus, we have $S^a_R = 1$, if either G'_t or G^*_t is stable. And \mathcal{V}^a_R accounts for the occupied volume of the bimanual system. Fig. 9 demonstrates the robots building a Lego faucet following the planned assembly sequence.

V. DISCUSSION

1) *Action masking*: Correct action masking is important in solving ASP. In applications where a reliable physics engine is available, we can use the simulator to guide the ASP. However, when a simulator is unavailable, it is important to

¹To better illustrate the usage of different bricks, we use one color for one type of brick when displaying the real assembly. 1×1 : purple. 1×2 : orange. 1×4 : blue. 1×6 : yellow. 1×8 : red. 2×2 : beige. 2×4 : black. 2×6 : red.

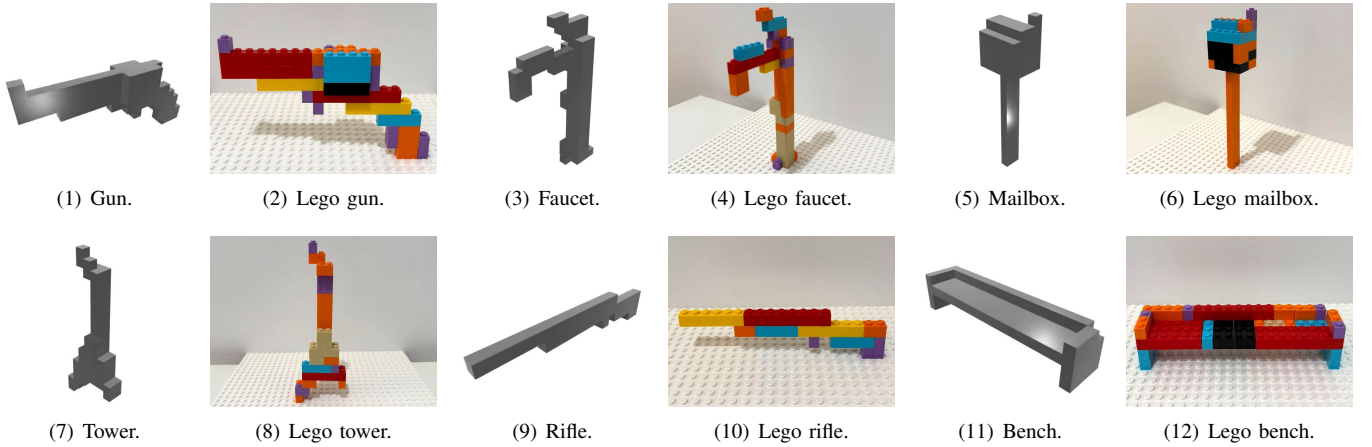


Fig. 6: Examples of 3D shapes in StableLego and their real assemblies. Top row: structures from StableLego. Bottom row: structures from Hard StableLego.

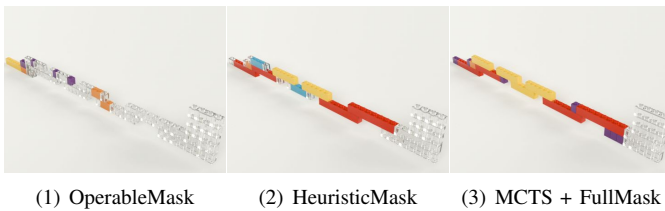


Fig. 7: Failure examples. Transparent bricks: unfinished shape.

design correct action masking to align the computation to real-world physics. Fig. 7 illustrates failures from the baselines for planning the shape in Fig. 4(3). Fig. 7(1) illustrates the failure of the OperableMask. Since it does not consider structural stability, it places floating bricks. Despite considering stability by heuristic, the HeuristicMask fails as shown in Fig. 7(2) due to the sim-to-real gap and the structure collapses in real. By integrating the FullMask, the MCTS + FullMask plans physically valid assembly actions. However, it fails as shown in Fig. 7(3) due to the sub-optimal long-horizon planning and enters a dead-end, where no further action is available.

2) *Computation Time*: The majority of the computation time is due to the stability analysis in Eq. (7) when computing the action mask. As a reference, the baselines take $< 0.1s$ to compute the action mask whereas ours takes $\sim 0.2s$, and longer when having larger assemblies.

3) *RL vs MCTS*: The inference time for our method is approximately $0.2s/step$, whereas the MCTS + FullMask takes around $15s/step$ due to the simulation steps when making a decision. However, MCTS is training-free, whereas ours takes 30-60min to learn for the example in Fig. 4(3). There is a clear tradeoff between training time and inference performance. Fig. 8 compares the exploration spaces between MCTS + FullMask (top) and ours (bottom). We can see that the RL framework leads to a wider and deeper exploration space, and thus, a better performance in planning assembly sequences.

4) *Extension*: In addition to Lego assembly, the proposed action mask can be easily extended to other combinatorial block assemblies such as block stacking, industrial palletization, etc. Fig. 10 illustrates a block stacking example. The action mask in Eq. (8) can be directly adopted simply by reducing the friction capacity between block connections [26]. To construct the target structure shown in the right, the

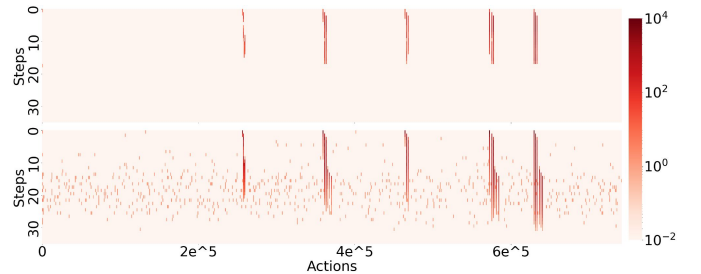


Fig. 8: Comparison of the exploration spaces between MCTS + FullMask (top) and ours (bottom). The darker color indicates more frequent visits.

physics-aware action mask can reliably prune the infeasible actions and guide the planning.

5) *Limitations and Future Works*: First, as mentioned in Sec. V-2 and V-3, the computation time for the action mask is non-trivial and accounts for 60 – 70% of the total time. Thus, we aim to improve the mask inference time by leveraging the action mask to learn an NN-based action mask to improve the computation time. Second, this work focuses on designing an effective action mask for solving ASP, thus, the policy model structure is not tuned. In the future, we aim to improve the policy structure (*e.g.*, network size, graph representation, etc) and make the assembly policy more generalizable to unseen 3D shapes, building an ASP generalist that can plan for any voxel input with any inventory. Third, the current method plans a step-by-step assembly sequence, which could fail when a valid assembly sequence does not exist for a structure. In the future, we would like to explore hierarchical assembly strategies, which could improve the planning capability for more diverse structures.

VI. CONCLUSION

This paper studies ASP for physical combinatorial block assembly. To address the combinatorial nature and ensure the physical validity of the planned assembly sequence, we employ deep reinforcement learning to learn a construction policy and design an online physics-aware action mask that effectively filters out invalid actions and guides policy learning. We demonstrate that the proposed method can successfully plan physically valid assembly sequences for constructing different 3D structures.

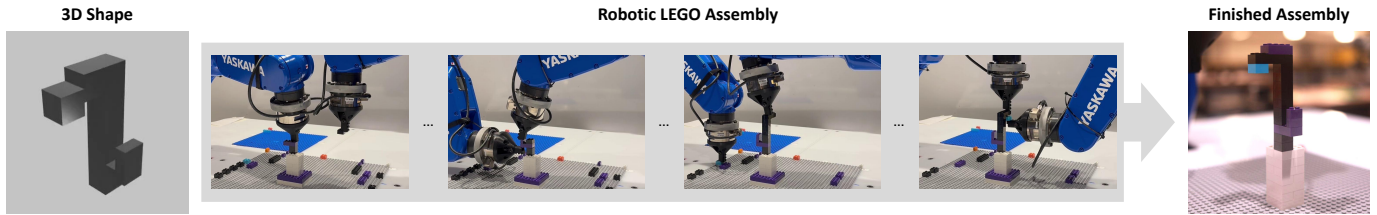


Fig. 9: A bimanual robotic system executing the planned assembly sequence.

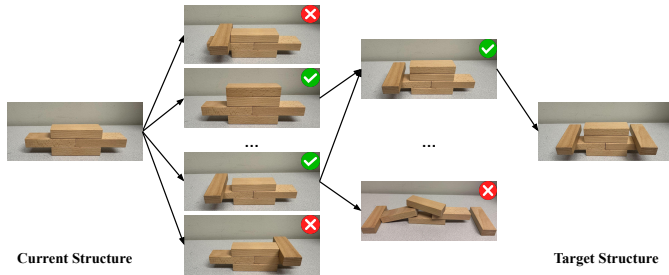


Fig. 10: Examples of applying the proposed action mask to block stacking/palletization.

REFERENCES

- [1] R. Liu, A. Chen, X. Luo, and C. Liu, “Simulation-aided learning from demonstration for robotic lego construction,” *arXiv preprint arXiv:2309.11010*, 2023.
- [2] R. Liu, R. Chen, A. Abuduweili, and C. Liu, “Proactive human-robot co-assembly: Leveraging human intention prediction and robust safe control,” in *2023 IEEE Conference on Control Technology and Applications (CCTA)*, 2023, pp. 339–345.
- [3] S.-J. Luo, Y. Yue, C.-K. Huang, Y.-H. Chung, S. Imai, T. Nishita, and B.-Y. Chen, “Legolization: Optimizing lego designs,” *ACM Trans. Graph.*, vol. 34, no. 6, nov 2015.
- [4] H. Chung, J. Kim, B. Knyazev, J. Lee, G. W. Taylor, J. Park, and M. Cho, “Brick-by-Brick: Combinatorial construction with deep reinforcement learning,” in *Advances in Neural Information Processing Systems (NeurIPS)*, vol. 34, 2021.
- [5] Z. Wu, Y. Li, W. Zhan, C. Liu, Y.-H. Liu, and M. Tomizuka, “Efficient reinforcement learning of task planners for robotic palletization through iterative action masking learning,” *IEEE Robotics and Automation Letters*, vol. 9, no. 11, pp. 9303–9310, 2024.
- [6] E. Danahy, E. Wang, J. Brockman, A. Carberry, B. Shapiro, and C. B. Rogers, “Lego-based robotics in higher education: 15 years of student creativity,” *International Journal of Advanced Robotic Systems*, vol. 11, no. 2, p. 27, 2014.
- [7] C. Zhou, B. Tang, L. Ding, P. Sekula, Y. Zhou, and Z. Zhang, “Design and automated assembly of planetary lego brick for lunar in-situ construction,” *Automation in Construction*, vol. 118, p. 103282, 2020.
- [8] A. C. Sanderson, L. S. Homem de Mello, and H. Zhang, “Assembly sequence planning,” *AI Magazine*, vol. 11, no. 1, p. 62, Mar. 1990.
- [9] Y. Lee, E. S. Hu, and J. J. Lim, “Ikea furniture assembly environment for long-horizon complex manipulation tasks,” in *2021 IEEE International Conference on Robotics and Automation (ICRA)*, 2021, pp. 6343–6349.
- [10] P. Culbertson, S. Bandyopadhyay, and M. Schwager, “Multi-robot assembly sequencing via discrete optimization,” in *2019 IEEE/RSJ International Conference on Intelligent Robots and Systems (IROS)*, 2019, pp. 6502–6509.
- [11] Y. Tian, J. Xu, Y. Li, J. Luo, S. Sueda, H. Li, K. D. Willis, and W. Matusik, “Assemble them all: Physics-based planning for generalizable assembly by disassembly,” *ACM Trans. Graph.*, vol. 41, no. 6, 2022.
- [12] K. Nagpal and N. Mehr, “Optimal robotic assembly sequence planning (orasp): A sequential decision-making approach,” in *2024 IEEE/RSJ International Conference on Intelligent Robots and Systems (IROS)*, 2024, pp. 9847–9854.
- [13] S. K. S. Ghasemipour, S. Kataoka, B. David, D. Freeman, S. S. Gu, and I. Mordatch, “Blocks assemble! learning to assemble with large-scale structured reinforcement learning,” in *International Conference on Machine Learning*. PMLR, 2022, pp. 7435–7469.
- [14] M. Atad, J. Feng, I. Rodríguez, M. Dürner, and R. Triebel, “Efficient and feasible robotic assembly sequence planning via graph representation learning,” in *2023 IEEE/RSJ International Conference on Intelligent Robots and Systems (IROS)*, 2023, pp. 8262–8269.
- [15] L. Ma, J. Gong, H. Xu, H. Chen, H. Zhao, W. Huang, and G. Zhou, “Planning assembly sequence with graph transformer,” in *2023 IEEE International Conference on Robotics and Automation (ICRA)*. IEEE, 2023, pp. 12 395–12 401.
- [16] X. Luo, S. Xu, R. Liu, and C. Liu, “Decomposition-based hierarchical task allocation and planning for multi-robots under hierarchical temporal logic specifications,” *IEEE Robotics and Automation Letters*, vol. 9, no. 8, pp. 7182–7189, 2024.
- [17] R. Lipsh-Sokolik, O. Khersonsky, S. P. Schröder, C. de Boer, S.-Y. Hoch, G. J. Davies, H. S. Overkleeft, and S. J. Fleishman, “Combinatorial assembly and design of enzymes,” *Science*, vol. 379, no. 6628, pp. 195–201, 2023.
- [18] V. Bapst, A. Sanchez-Gonzalez, C. Doersch, K. Stachenfeld, P. Kohli, P. Battaglia, and J. Hamrick, “Structured agents for physical construction,” in *International conference on machine learning*. PMLR, 2019, pp. 464–474.
- [19] R. P. Testuz, Y. Schwartzburg, and M. Pauly, “Automatic generation of constructible brick sculptures,” Tech. Rep., 2013.
- [20] D. Silver, A. Huang, C. J. Maddison, A. Guez, L. Sifre, G. Van Den Driessche, J. Schrittwieser, I. Antonoglou, V. Panneershelvam, M. Lanctot *et al.*, “Mastering the game of go with deep neural networks and tree search,” *nature*, vol. 529, no. 7587, pp. 484–489, 2016.
- [21] J. B. Hamrick, V. Bapst, A. Sanchez-Gonzalez, T. Pfaff, T. Weber, L. Buesing, and P. W. Battaglia, “Combining q-learning and search with amortized value estimates,” in *International Conference on Learning Representations*, 2020.
- [22] T. Chabal, R. Strudel, E. Arlaud, J. Ponce, and C. Schmid, “Assembly planning from observations under physical constraints,” in *2022 IEEE/RSJ International Conference on Intelligent Robots and Systems (IROS)*. IEEE, 2022, pp. 10 223–10 229.
- [23] N. Funk, G. Chalkatzaki, B. Belousov, and J. Peters, “Learn2assemble with structured representations and search for robotic architectural construction,” in *5th Annual Conference on Robot Learning*, 2021.
- [24] J. Kim, H. Chung, J. Lee, M. Cho, and J. Park, “Combinatorial 3D shape generation via sequential assembly,” *arXiv preprint arXiv:2004.07414*, 2020.
- [25] S. Huang and S. Ontañón, “A closer look at invalid action masking in policy gradient algorithms,” *arXiv preprint arXiv:2006.14171*, 2020.
- [26] R. Liu, K. Deng, Z. Wang, and C. Liu, “Stablelego: Stability analysis of block stacking assembly,” *IEEE Robotics and Automation Letters*, vol. 9, no. 11, pp. 9383–9390, 2024.
- [27] A. Raffin, A. Hill, A. Gleave, A. Kanervisto, M. Ernestus, and N. Dornmann, “Stable-baselines3: Reliable reinforcement learning implementations,” *Journal of Machine Learning Research*, vol. 22, no. 268, pp. 1–8, 2021.
- [28] J. Schulman, F. Wolski, P. Dhariwal, A. Radford, and O. Klimov, “Proximal policy optimization algorithms,” *arXiv preprint arXiv:1707.06347*, 2017.
- [29] R. Liu, Y. Sun, and C. Liu, “A Lightweight and Transferable Design for Robust Lego Manipulation,” *International Symposium on Flexible Automation*, 2024.
- [30] P. Huang, R. Liu, S. Aggarwal, C. Liu, and J. Li, “Apex-mr: Multi-robot asynchronous planning and execution for cooperative assembly,” *arXiv preprint arXiv:2503.15836*, 2025.